IET Radar, Sonar & Navigation

Research Article

IET Journals
The Institution of Engineering and Technology

Compatibility problems related with pulse-compression, solid-state marine radars

ISSN 1751-8784
Received on 24th July 2015
Revised on 12th October 2015
Accepted on 16th November 2015
doi: 10.1049/iet-rsn.2015.0400
www.ietdl.org

Gaspare Galati ✉, *Gabriele Pavan*, *Francesco De Palo*

Department of Electronic Engineering, Tor Vergata University, via del Politecnico 1, Rome, Italy
✉ *E-mail: gaspare.galati@uniroma2.it*

Abstract: The better and better attention being paid to the primary resources (especially oil and raw materials) and the increasing environmental consciousness are among the main drivers of the growth of vessel traffic, also because sea shipping has a good delivery rate and affordable operating costs in comparison with other transport means. In such a frame, an effective and efficient vessel traffic requires tight control and adequate navigation aids in order to ensure safety, reduction of risks for the environment, as well as efficient, quick and comfortable navigation. This study deals with the evolution of the marine (navigation) radar systems from the point of view of the potential drawbacks due to the implementation of solid-state (SS) technology (and the subsequent pulse compression) in the incoming, new generation, SS marine radars. The authors found that the high duty cycle of these incoming SS marine radar sets will generate severe interference to all marine radar sets in visibility with a significant reduction, well below the international regulations, of their detection capability. Mitigation of these damaging effects is not an easy task, subject of further research.

1 Introduction

The diffusion of marine radar-based surveillance systems and the pertaining regulations go back to the 1970's when the International Maritime Organization (IMO) issued the 'International Convention for the Safety Of Life At Sea' (SOLAS) which is the most important international treaty concerning the safety of ships [1]. The autonomous decision of manoeuvring a ship is delegated to its captain in compliance with the international navigation rules; however, for areas covered by a vessel traffic system (VTS), the crew may receive directly, from the authorities in charge, the directions on the route to follow. Moreover, thanks to the non-cooperative surveillance and navigation system based on radar system, and to the cooperative one installed on board, i.e. the automatic identification system (AIS) based on GPS data, it is possible to get an overall picture of the nearby maritime traffic.

Even in the Global Navigation Satellite System (GNSS) era, the on-board radar sensor remains of fundamental importance to avoid obstacles such as non-cooperating (e.g. small) vessels and to visually acquire the coastline and the islands. Based on the IMO regulations [2, 3], the main characteristics of marine radars are frequency band from 9300 to 9500 MHz in the X-band and 2900–3100 MHz in the S-band, and for the acceptable values (worst case): range accuracy 30 m, angular accuracy 1°, range resolution 40 m, azimuthal resolution 2.5°, minimum distance of detection from 5 nm for small ships to 20 nautical miles (nm) for high coasts (60 m), probability of detection 0.8 and probability of false alarm 10^{-4}.

The traditional marine radar systems are based on the low-cost commercial *magnetron* (MG) technology with relatively high peak power levels (up to 25–50 kW) [4] and a small duty cycle whose order of magnitude is $2 \times 10^{-4} \div 7 \times 10^{-4}$. The simplicity and low cost of these MG radars are, unfortunately, associated with the short life of the MGs themselves – of the order of one (or a few) thousand hours – calling for a frequent and expensive maintenance.

In recent years, a new generation of marine radar is being developed using the solid-state (SS) transmitter technology. These radar systems have a lower cost of maintenance with mean time between failures of the order of 50,000 h and no high voltage circuitry. These systems work with low peak power levels (hundreds of W) using pulse compression (coded pulse in transmission and matched filter in reception) with a variable duty cycle up to about 10%. A basic drawback of the use of 'long pulse', i.e. high duty cycle, has been known for many years, but not yet seriously considered till now, excluding a single paper [5] (Section VII p. 163) where it is clearly stated: '*the interference effects that such a radar might cause on existing marine radars may be catastrophic*'. These effects become critical when the traffic density (number of ships per nm^2) increases. Although SS marine radars still have minimal diffusion for the main suppliers, they are expected to represent a future solution for marine radar systems because several companies are introducing them on the market. For this reason, it is very interesting *to study the damaging effects of the mutual interferences among different marine radars*, a topic which, in our opinion, has not received enough attention till today.

The aim of this paper is to evaluate the reduction of detection capability when more radars operate in mutual visibility conditions. This study starts from the definition of a statistical model for the distance between pairs of radars, derived using real data.

1.1 Main characteristics of marine radars

Table 1 reports the main parameters of marine radar with MG and SS technologies used in this paper for the evaluation of the probability of detection. While for MG radars the parameters, i.e. τ (pulse width), PRF (pulse repetition frequency) and *duty cycle* ($d = \tau \times \text{PRF}$) are relatively stable and well defined by the manufacturers, for SS radars, using *pulse compression*, the pulse length and the chirp-bandwidth are significantly varying from manufacturer to manufacturer. Typically the codified pulse length is from a few microseconds up to 100 µs, while the chirp-bandwidth is of the order of tens of MHz. Different types of pulse for short, medium and long ranges are transmitted in bursts with a burst repetition rate varying from 500 to 2000 Hz, range and mode dependent.

2 Radar visibility

The visibility between a pair (k, i) of ships occurs when the distance of their radar antennas is less than their 'horizon' $R_{ki} = R_k + R_i$, where

Table 1 Main parameters of some typical X-band marine radar

	MG	SS
Frequency	9410 ± 30 MHz	9300÷9500 MHz
Power	10, 12 and 25 kW	25, 50, 100 and 200 W
antenna length	4 ft (1.22 m), 6 ft (1.83 m), 8 ft (2.44 m)	6 ft (1.83 m), 9 ft (2.75 m) 12 ft (3.65 m)
beamwidth θ_{Az} (−3 dB)	1.8°, 1.2°, 0.95°	1.2°, 0.95°, 0.65°
beamwidth θ_{El} (−3 dB)	20°÷24°	22° ÷ 25°
τ [μs]/PRF [Hz] short pulse	0.055/3000	0.05/3000 without compression
τ [μs]/PRF [Hz] medium pulse	0.2/1500	32/1500 with pulse compression[a]
τ [μs]/PRF [Hz] long pulse	1.2/600	64/800 with pulse compression
duty cycle short pulse	0.0165%	0.0165%
duty cycle medium pulse	0.03%	4.8%
duty cycle long pulse	0.072%	5.12%
rotation speed ω	24/48 rpm	24/48 rpm
receiver band	20 MHz (short, medium) 4 MHz (long)	chirp bandwidth: 2–32 MHz
noise figure	<6 dB	5 dB
MTBF	<5000 h (typical)	> 50,000 h

[a]With pulse compression the chirp length is typically up to 100 μs with chirp-bandwidth of tens MHz; generally chirp pulses are transmitted in a burst with burst repetition rate of 500–2000 Hz, range and mode dependent. Typically the effective pulse compression ratio is <150 in all modes

R_k (resp. R_i) is the 'radar horizon' of the kth (resp. ith) ship [6]. The *visibility distance* R_{ki}, depending on the antenna heights h_k and h_i, using the equivalent earth radius $r_e \cong 8500$ km in standard atmosphere, can be evaluated as [6]

$$R_{ki} \cong \sqrt{2r_e} \cdot \left(\sqrt{h_k} + \sqrt{h_i}\right) \quad (1)$$

Unfortunately, the radar antenna height above sea level is not a part of the vessel-derived AIS information. Therefore, in this study, this parameter had to be empirically estimated for each class of ship (passenger, cargo, tanker, fishing etc.) by relating it to the ship length (available in the AIS message) using specialised websites [7–9]. Considering 13 classes for the ships (see Table 2), 10 samples for each class, 130 samples have been used to derive a non-linear regression (see Fig. 1) to evaluate h (m) against the ship length x (m)

$$h = 0.7825 \cdot x^{0.728} \quad (2)$$

2.1 Marine areas

In collaboration with the General Command of the Italian Coast Guard, six areas of maritime traffic have been identified in the Mediterranean Sea: (i) Central Adriatic, (ii) Otranto Canal, (iii) Central Tyrrhenian (near Naples), (iv) Messina Strait, (v) Canal of Sicily and (vi) Dardanelles/Bosporus. For the week: 23 February–1 March 2015, each area was sampled at regular intervals of 4 h, i.e. at 00:00, 04:00, 08:00, 12:00, 16:00, 20:00. Finally, the total number of vessels and the density of ships in route have been evaluated. The largest values are shown in Table 3. The large number of ships in area (1) – Central Adriatic, early morning – is due to the very intense fishing activities.

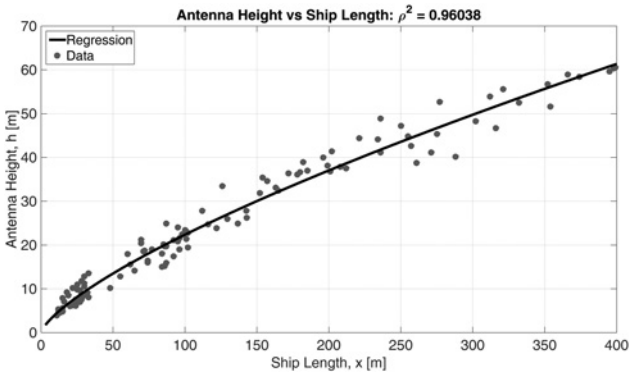

Fig. 1 *Antenna height (m) against ship length (m)*

Table 3 Density of maritime traffic

Area	Date/time	Ships	Density [units of 10^{-3} ships/nm^2]		
			Enroute	In harbour	Total
(1) Central Adriatic	Tuesday, 24/02/15, 04:00	285	20.88	1.76	22.65
(2) Otranto Canal	Tuesday, 24/02/15, 08:00	46	3.74	0.98	4.72
(3) Central Tyrrhenian	Friday, 27/02/15 08:00	45	6.72	4.03	10.75
(4) Messina Strait	Friday, 27/02/15 16:00	73	5.40	2.41	7.81
(5) Canal of Sicily	Friday, 27/02/15 08:00	104	4.56	0.39	4.96
(6) Dardanelles/ Bosporus	Thursday, 26/ 02/15 12:00	53	2.44	0.51	2.95

2.2 Statistical model for the mutual distance between ships

Considering the number of observed vessels in each area, a statistical model for the mutual distance between a pair of ships has been estimated. Generally, it depends on the observed marine area, but

Table 2 Antenna height of different types of ships: mean and standard deviation σ

No.	IMO number	Ship type	Length		Antenna height		Radar horizon, nm
			Mean, m	σ, m	Mean, m	σ, m	
1	50	pilot	14	2	5	1.2	5.0
2	30	fishing	26	4	7	1.0	5.9
3	37	yacht (<30 m)	27	3	8	1.6	6.3
4	31/32/51	towboat	25	5	10	1.9	7.0
5	40 ÷ 49	high speed craft	82	15	16	2.0	8.9
6	37	yacht (>30 m)	81	20	20	5.4	10.0
7	60 ÷ 69	passengers (<150 m)	96	32	22	5.0	10.4
8	55	military	100	39	23	7.7	10.7
9	70 ÷ 79	cargo	112	29	24	4.8	10.9
10	60 ÷ 69	passengers (>150 m)	177	25	36	4.0	13.3
11	80 ÷ 89	tanker (<250 m)	206	40	40	6.0	14.1
12	80 ÷ 89	tanker (>250 m)	291	34	45	5.0	15.0
13	70 ÷ 79	container	337	68	56	6.4	16.6

IET Radar Sonar Navig., 2016, Vol. 10, Iss. 4, pp. 791–797

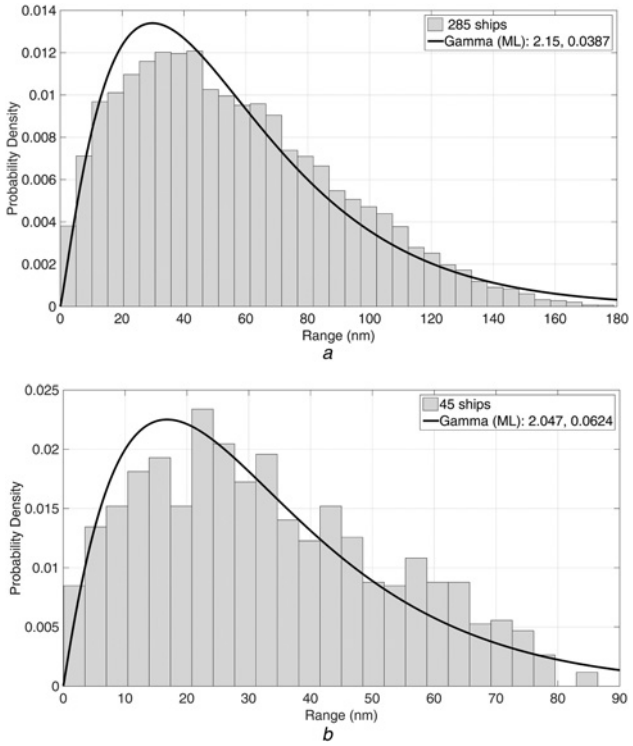

Fig. 2 *Histogram and estimated probability density (gamma) of the mutual distance between a pair of ships*

a Area (1) Central Adriatic
b Area (3) Central Tyrrhenian (near Naples)

a gamma model is well suited to most data sets

$$f_R(r) = \frac{\lambda^b}{\Gamma(b)} r^{b-1} \mathrm{e}^{-\lambda r}, \quad r > 0 \tag{3}$$

The parameters (λ, b) have been estimated by the maximum-likelihood method [10]. Fig. 2 shows the histogram and the gamma density function for area (1) where $\lambda = 2.15$ and $b = 0.0387$ and for area (3) where $\lambda = 2.047$ and $b = 0.0624$.

2.3 Probability of visibility among ships

We have shown that the distance R_{ki} between two ships (k, i) can be modelled by a random variable R with a gamma density function and that a type 'k' ship *sees* a ship of type 'i' when $R_{ki} \le R_k + R_i$. Hence, indicating with P_i the probability that the ship be of type $i = 1, \ldots, N_{\text{type}}$, the probability of visibility is

$$P(\text{vis})_{k,i} = \text{Prob}\{R_{ki} < R_k + R_i\} \cdot P_i \tag{4}$$

Generalising, the probability $P(\text{vis})_k$ that the ship 'k' sees any type of ship becomes

Table 4 Probability of visibility

Area	Most frequent ship type	Antenna height, m	P_i, %	P (vis)$_k$, %	P (vis), %
(1) Central Adriatic	cargo	24	6	11.7	7.2
	fishing	7	88	6.5	
(2) Otranto Canal	cargo	24	30	26.3	25.9
	fishing	7	30	19.9	
(3) Central Tyrrhenian	passenger	22	20	31.4	27.7
	fishing	7	44	21.8	
(4) Messina Strait	cargo	24	33	14.4	14.5
	tanker	45	15	18.3	
(5) Canal of Sicily	cargo	24	20	17.7	15.0
	fishing	7	60	11.6	
(6) Dardanelles/ Bosporus	cargo	24	43	21.3	21.0
	tanker	45	25	25.1	

$$P(\text{vis})_k = \sum_{i=1}^{N_{\text{type}}} P(\text{vis})_{k,i} = \sum_{i=1}^{N_{\text{type}}} \gamma(b, \lambda, x) \cdot P_i \tag{5}$$

with $x = \lambda(R_k + R_i)$ and $\gamma(b, \lambda, x) = (1/\Gamma(b)) \int_0^x e^{-t} t^{b-1}\, \mathrm{d}t$ are the *incomplete gamma functions* [11]. Varying k, the probability that *any pair of ships* be in visibility (*probability of visibility*) is

$$P(\text{vis}) = \sum_{k=1}^{N_{\text{type}}} P(\text{vis})_k \cdot P_k \tag{6}$$

For each area, Table 4 reports the probability P_i of the pair of most frequent ships and, by (5) and (6), the probability of visibility. Although area (1) shows the highest density of traffic, the resulting probability of visibility is only 7.2%, as in this area 88% of the ships are fishing vessels, with a limited antenna height.

2.4 Comparison between data and model

Table 5 shows the number of '*enroute*' ships (i.e. excluding the tied up ones) and the number of the radar in visibility for each area; in the last column the 50th percentile is shown. It results that, in areas (1) and (3), the maximum number of vessels that a given ship *sees* is 48 and 24, respectively, with an empirical mean of 21.37 and 10.71. Using the probability of visibility [remember that for area (1) P (vis) = 0.072], and considering the number of ships at sea [i.e. 285 in area (1)], the resulting mean value is 20.52 which is very close to the measured one, i.e. 21.37.

Area (3) shows a moderate traffic : 45 ships with a density of 6.72×10^{-3} ships/nm^2, 44% of which being fishing ships, i.e. with limited antenna height, and 41% being large vessels (cargo, passengers, tankers) with a much higher antenna. Multiplying the probability of visibility (0.277) by the number of ships *enroute* (45), the mean value results equal to 12.46, i.e. a bit larger than the empirical one (10.71).

3 Probability of detection

To evaluate the effects of the interferences on the probability of detection, we define (Fig. 3) the *time of overlap* T_{over} as the interval $\tau_i + \tau_k$ with no interfering pulses, where τ_k and τ_i are the

Table 5 Number of ships in visibility

Area	Ships enroute	Max	Min	Ave (data)	Ave (model)	Dev. std.	50° percentile
(1) Central Adriatic	285	48	2	21.37	20.52	10.75	20
(2) Otranto Canal	46	28	0	10.73	11.91	6.53	11
(3) Central Tyrrhenian	45	24	1	10.71	12.46	6.67	12
(4) Messina Strait	73	21	0	10.58	10.73	6.04	6
(5) Canal of Sicily	104	32	2	12.71	15.6	6.08	12
(6) Dardanelles/Bosporus	53	22	0	10.72	11.13	8.40	6

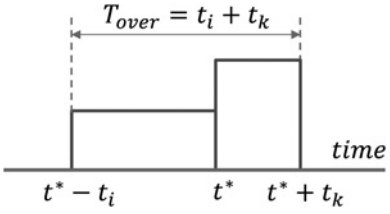

Fig. 3 *Time of overlap, T_{over}*

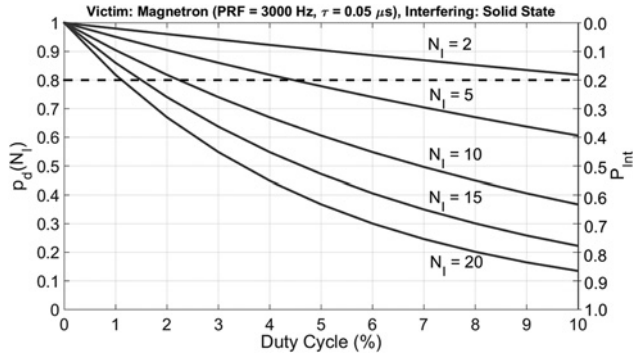

Fig. 4 *Probability of detection $p_d(N_I)$ (left axis) and probability of interference P_{Int} (right axis) against the SS radar duty cycle, varying the number of interfering ships. Victim is an MG radar, interfering ships are all of the SS type, $p_d(N_I = 0) = 1$*

pulse widths of the ship '*k*' (*victim*) and of the ship '*i*' (*interfering*) radars and *t** is the leading edge of the '*victim*' radar pulse.

The probability that *n* interfering pulses with repetition frequency PRF_i fall into the interval T_{over} (independent radar operation is assumed) is obtained by the Poisson law

$$p_i(n) = \frac{(\mathrm{PRF}_i \cdot T_{\mathrm{over}})^n}{n!} e^{-\mathrm{PRF}_i \cdot T_{\mathrm{over}}} \tag{7}$$

Supposing that in an ideal condition (no noise, no clutter) the '*single hit*' probability of detection p_{d} be very close to one, then in the presence of N_I interfering pulses p_{d} decreases as

$$p_{\mathrm{d}}(N_I) = \prod_{i=1}^{N_I} p_i(n=0) = \exp\left[-\sum_{i=1}^{N_I} \mathrm{PRF}_i \cdot T_{\mathrm{over}}\right] \tag{8}$$

When roughly speaking, $N_I < 40$, if all interfering ships are SS type with same duty cycle (d_I), $\mathrm{PRF}_i = 1000$ Hz and τ is variable from 10 to 100 μs (d_I up to 10%), or conversely, for the MG radar $\tau = 0.05$ μs,

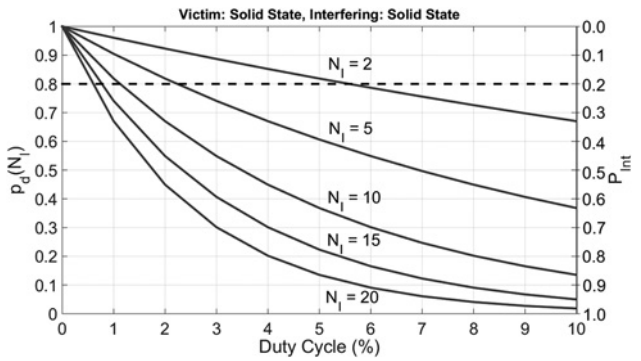

Fig. 5 *Probability of detection $p_d(N_I)$ (left axis) and probability of interference P_{Int} (right axis) against the SS radar duty cycle, varying the number of interfering ships. Both victim and interfering radars are of the same SS type (and parameters), $p_d(N_I = 0) = 1$*

(8) can be simplified as

$$p_{\mathrm{d}}(N_I) \cong \exp\left[-a \cdot N_I \cdot d_I\right] \tag{9}$$

with $a = 1$ when the victim radar is an MG type, and $a = 2$ when the victim is a SS type.

Figs. 4 and 5 show the reduction of the probability of detection, $p_{\mathrm{d}}(N_I)$, due to the interference when the victim radar is an MG type and a SS one, respectively.

The number of the interfering ships is $N_I = 2, 5, 10, 15, 20$. The axis on the right side shows the *probability of interference*: we call *probability of interference* P_{Int} the probability of at least one interfering pulse in the interval T_{over}, i.e. the complement to the unit of (8). From these figures, it results that a few interfering ships, also for a low duty cycle, drastically reduce p_{d} under the IMO limit of 0.8, especially when the victim is a SS radar (Fig. 5).

However, in (8) and (9) we have supposed that all marine radars (both victim and interfering) transmit in the same band. Table 1 shows for MG radars a band of 9410 MHz ± 30 MHz (practically implemented by all manufacturers, the '*historical*' band of 9375 MHz being less and less used), while for SS radar the extent of use of the band from 9300 to 9500 MHz depends on the manufacturers. A first example, i.e. a SS marine radar on the civil ships market, uses a transmitted peak power of 25 W, occupying *circa* 100 MHz of band for the six pulses with different chirp lengths (short, medium and long), a central frequency and a band occupancy (in MHz) of 9410 (±16), 9438 (±16), 9450–9470 (±8), 9466–9486 (±4.7), 9486–9490 (±2) and 9486–9495 (±1). A second example of a radar on the market (a VTS radar) shows a transmitted peak power of 200 W, with central frequencies varying from 9166 to 9465 MHz with 35 MHz of band for long (40 μs), medium (15 μs) and short (150 ns) chirp length. Concluding, each of these new SS marine (or VTS) radars *tend to occupy the whole marine band*. In one case, the installation of two radar sets on a leisure boat has been proposed, i.e. a low power, continuous wave radar with a very short minimum range (not limited by the pulse duration as in pulsed radars) and a SS radar with a large maximum range: the whole 9300–9500 MHz band is practically occupied by this pair of radar sets.

A future ideal band allocation to separate the MG band from the SS one may be similar to the one shown in Fig. 6 where we have supposed four different bands ($S_1 = S_4 \Rightarrow 20$ MHz, $S_2 = S_3 \Rightarrow 30$ MHz) for SS radar with four guard bands. In this way the waveforms of MG systems are always orthogonal (separated in frequency) to the SS ones.

By this last consideration, we can modify (8) as follows

$$p_{\mathrm{d}}(N_I) = \prod_{i=1}^{N_I} p_i(n=0) = \exp\left[-\sum_{i=1}^{N_I} \mathrm{PRF}_i \cdot T'_{\mathrm{over}}\right] \tag{10}$$

where $T'_{\mathrm{over}} = (\tau_i + \tau_k) \cdot \delta_{ik}$ being $\delta_{ik} = 1$ if the transmitted frequencies of the ships *i* and *k* are equal ($f_i = f_k$) and $\delta_{ik} = 0$ otherwise. To quantify this situation, we assume the following: (*a*) $\delta_{ik} = 1$ if the victim and the interfering radars are MG type, (*b*) $\delta_{ik} = 0$ if the SS radars never use the MG frequencies, (*c*) $\delta_{ik} = 1$ if the victim and the interfering radars are of the SS type in 25% of cases, supposing a uniform distribution for the use of the four bands. Hence, the effective number of interfering ships is reduced to one-fourth and (9) becomes (with $a = 2$)

$$p_{\mathrm{d}}(N_I) \cong \exp\left[-\frac{1}{2} N_I \cdot d_I\right] \tag{11}$$

The use of the four bands as defined in Fig. 6 permits to remove interferences (between MG and SS apparatus) and to reduce the mutual interferences among the SS radars. The improvement in terms of duty cycle corresponds to the number of sub-bands in which the total allocated band for marine radar (200 MHz) is divided.

Note that detection and false alarm probabilities as evaluated beforehand do not include the effect of the azimuthal integration

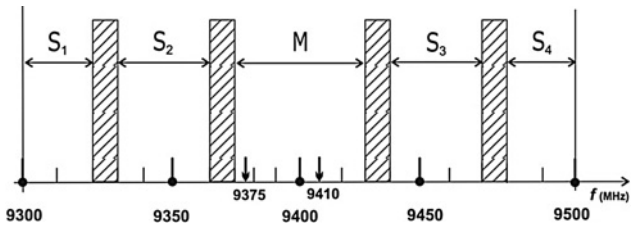

Fig. 6 *Ideal band occupancy for MG (M) and SS marine radars (S_1, S_2, S_3, S_4)*

of pulses (i.e. the extractor), which will be discussed in the following section. Moreover, the '*raw*' assumption was made that any interfering pulse '*blanks*' the overlapped valid pulse, neglecting the analysis of more or less sophisticated constant false alarm rate systems, while the more relevant effects of azimuthal integration are analysed in the following.

4 Azimuthal integration of pulses and binary moving window extractor

The main antenna parameters for marine radars (excluding the long-range, coastal VTS radars) are shown in Table 1. The –3 dB azimuth beamwidth θ_{Az} (degrees) and the rotation speed ω (rpm) permit to evaluate the dwell time t_D [6]

$$t_D = \frac{\theta_{Az}(\text{degrees})}{6 \cdot \omega(\text{rpm})} \quad [\text{s}] \tag{12}$$

With the operational value of the PRF, the number of azimuthal pulses available for integration is $N = \text{PRF} \cdot t_D$. Considering the range for θ_{Az}, ω and PRF, this number can vary from a few units to some tens (i.e. in most cases N ranges from 5 to 30 pulses).

The video integration of these 'reference', non-coherent radars is implemented in digital form using an A/D converter after the envelope detector. For the evaluations, we consider the simple case (widely used in the past for its ease of implementation) of a 1-bit converter, leading to a closed-form expression, i.e. the binomial law [12]. It corresponds to a threshold detector operating directly on the output of the envelope detector, followed by an accumulator which counts up to M '*hits*' out of N before generating an output decision (detection or false alarm). This is the well-known binary moving window, MW extractor [12]. In the case of noise alone the single hit probability of false alarm, p_{fa} (written in lowercase) at the input of the extractor is

$$p_{fa} = \exp\left[-\frac{T^2}{2}\right] \tag{13}$$

where the threshold T has been supposed normalised to the *rms* noise (square root of the noise power). Then the relationship between N, the detection thresholds (i.e. primary T and secondary M) and the probability of false alarm at the output of the extractor, P_{FA} (written in uppercase), is (binomial law)

$$P_{FA} = \sum_{k=M}^{N} \binom{N}{k} p_{fa}^{k} \cdot \left(1 - p_{fa}\right)^{N-k} \tag{14}$$

For each M, fixing P_{FA}, for example 10^{-6}, the probability p_{fa} is evaluated by (14) and the threshold T is estimated inverting (13). In the case of signal plus noise, the probability of detection on single hit, p_d (written in lowercase), depends on the target model. For a non-fluctuating (steady) target with a given signal-to-noise-ratio (SNR) it is [6]

$$p_d = \int_{T}^{+\infty} v \cdot \exp\left[-\frac{v^2}{2} - \text{SNR}\right] I_0\left(v\sqrt{2 \cdot \text{SNR}}\right) \, dv \tag{15}$$

where $I_0(\cdot)$ is the modified Bessel function of the first kind. For a fluctuating target (Swerling 2)

$$p_d = \exp\left[-\frac{T^2}{2(1 + \text{SNR})}\right] \tag{16}$$

At the output of the extractor, the probability of detection, P_D (in uppercase), is given by

$$P_D = \sum_{k=M}^{N} \binom{N}{k} p_d^{k} \cdot \left(1 - p_d\right)^{N-k} \tag{17}$$

The optimum threshold M is chosen by minimising the SNR with fixed P_{FA} and P_D. Of course this way of integrating pulses causes losses with respect to a perfect (coherent) integrator exploiting the full dynamic range. For a steady target, $P_D = 0.9$ and $P_{FA} = 10^{-6}$, Table 6 shows the integration losses in addition to the coherent integration ones (data are obtained from [13] p. 65, Fig. 2.9).

The use of 1-bit only introduces an extra loss of $-1.6 \div -1.5$ dB (see Table 6), which may be accepted because 1-bit A/D conversion offers significant protection against interference from random pulses of large amplitude: no matter how large the interfering pulse is, it can only add '1' to the count of first-threshold crossings (see also the Appendix 1).

It has been shown in [12] that the optimum threshold M (which minimises the SNR), for a number of pulses of 10, 20 and 30, with $P_{FA} = 10^{-6}$, $P_D = 0.9$, are $M_{opt} = 6,\ 10,\ 14$, respectively, for a non-fluctuating target and $M_{opt} = 3,\ 5,\ 8$ for a fluctuating target (Swerling 2 model). When P_D is set to 0.99, M_{opt} becomes 7 when $N = 30$ (see Table 7).

The probability p_d in (17) should be not less than the values of Table 7, but with interference, i.e. when $P_{Int} > 0$, the p_d values decrease reducing the P_D and bringing it *below the IMO requirement of 0.8 also for a low probability of interference (less than 25%÷0.35%)* as shown in Fig. 7 for $P_D = 0.9$ and as in shown Fig. 8 for $P_D = 0.99$.

Substituting in (9) the probability $p_d(N_I)$ with $1 - P_{Int}$ and inverting this relationship, we get the relevant '*interference duty cycle*'

$$d_I = -\frac{1}{a \cdot N_I} \ln\left(1 - P_{Int}\right) \tag{18}$$

For a moving window with $N = 10,\ 20,\ 30$, reading in Figs. 7 and 8 the values of maximum P_{Int} when P_D reaches 0.8, we obtain (Table 8) the maximum acceptable probability of interference.

By (18), using the previous values of P_{Int}, the maximum (interference) duty cycle compatible with the IMO detection requirement can be evaluated as shown in Table 9 when the victim

Table 6 Comparison of losses ($P_D = 0.9$, $P_{FA} = 10^{-6}$) between video and moving window integration

N	Integration loss, dB		
	A: video	B: MW	B–A
10	1.9	3.4	1.5
20	2.9	4.5	1.6
30	3.5	5.1	1.6

Table 7 Probability at the input of the moving window: $P_D = 0.9(0.99)$, $P_{FA} = 10^{-6}$

N	Steady target			Swerling 2 target		
	M_{opt}	p_d	p_{fa}	M_{opt}	p_d	p_{fa}
10	6	0.73 (0.85)	0.042	3	0.45 (0.61)	0.0021
20	10	0.62 (0.72)	0.081	5	0.36 (0.48)	0.0094
30	14	0.57 (0.66)	0.110	8 (7)	0.32 (0.42)	0.0184

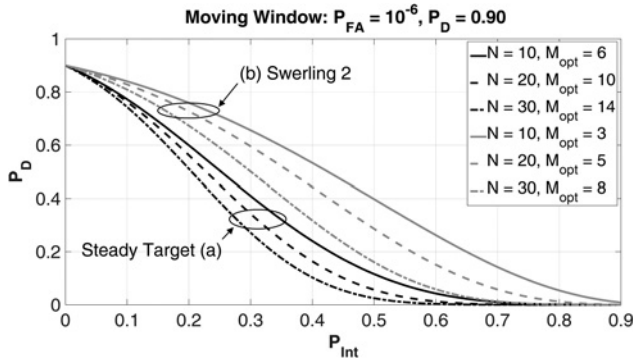

Fig. 7 *Probability of detection after binary integration against the probability of interference for N = 10, 20, 30 and the relevant values of M_{opt}, for $P_{FA} = 10^{-6}$, $P_D = 0.9$*

a Non-fluctuating target (steady target)
b Fluctuating target: Swerling 2

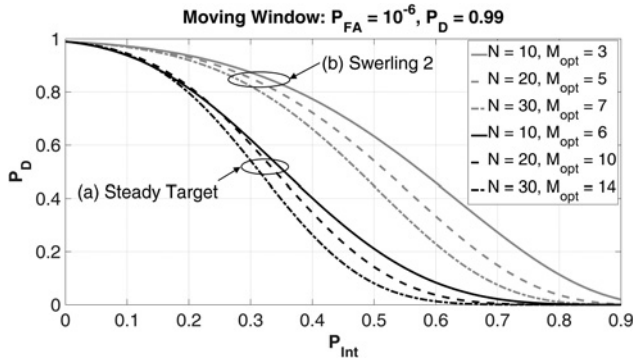

Fig. 8 *Probability of detection after integration against the probability of interference for N = 10, 20, 30 and the relevant values of M_{opt}, for $P_{FA} = 10^{-6}$, $P_D = 0.99$*

a Non-fluctuating target (steady target)
b Fluctuating target: Swerling 2

and interfering radars are a SS type [$a = 2$ in (18)] and the number of interfering ships is $N_I = 5$, 10, 15, 20 in the case of non-fluctuating target. For a fluctuating target the results are shown in Table 10. When the victim is an MG radar, i.e. $a = 1$ in (18), the duty cycle doubles.

It can be concluded that the presence of interferences, also with low probability, strongly reduces the probability of detection when most vessels will use SS radars unless their duty cycle is kept low, i.e. generally well below 1% and less than about 0.2% in high traffic as area (1), see first row of Tables 3 and 5. Only very strong targets (i.e. permitting $P_D \geq 0.99$) may be detected when the number of interfering ships is greater than about 10 (Table 5) and the duty cycle is above 1% (but anyway, <2.5%), see last row of Table 10. If in the future the proposed band occupancy (see Fig. 6) will be used, the values in Tables 9 and 10 would be increased by a fourfold factor (×4).

Table 8 Maximum P_{Int} for $P_D = 0.8$

	P_D	Maximum P_{Int}
steady target	0.90	0.08
	0.99	0.21
fluctuating target	0.90	0.15
	0.99	0.38

Table 9 Maximum duty cycle for $P_D = 0.8$, 'victim' SS, 'interfering' SS, non-fluctuating target

	$N_I = 5$	$N_I = 10$	$N_I = 15$	$N_I = 20$
$P_D = 0.90$	0.84%	0.42%	0.28%	0.21%
$P_D = 0.99$	2.36%	1.18%	0.79%	0.59%

Table 10 Maximum duty cycle for $P_D = 0.8$, 'victim' SS, 'interfering' SS, fluctuating target

	$N_I = 5$	$N_I = 10$	$N_I = 15$	$N_I = 20$
$P_D = 0.90$	1.50%	0.80%	0.50%	0.40%
$P_D = 0.99$	4.80%	2.40%	1.70%	1.30%

5 Comments and conclusions

The statistical analysis presented in this work has shown that the increasing diffusion of the SS marine radars might represent a critical problem for the sea traffic when the percentage of operating SS radars will reach a few percent, confirming what was reported seven years ago in [5].

Six areas of maritime traffic have been identified in the Mediterranean Sea and using the AIS (latitude, longitude) data a histogram of the distances between a pair of ships has been empirically evaluated observing that it fits with a gamma distribution with different parameters for each area. The use of gamma model leads to the probability of visibility P(vis), which is useful to evaluate the average number of interfering ships – about 20 – confirmed by the one taken from the empirical data (AIS).

We limited ourselves to consider the presence of interfering radar pulses (Poisson process) assuming that they simply negate the radar detection of overlapped, valid echo pulses, with no increase of the false alarm probability. This operating way is typical of the widely used '*interference blanking circuit*' implementing a logical AND between successive radar sweeps. With this assumption the effect on the 'victim' depends only on temporal parameters (pulse width and PRT) and the probability of interference P_{Int} is related to the number of vessels in visibility, to the PRF and to the sum of the pulse widths (interfered and interfering).

As a matter of fact, while in marine MG radars (having a duty cycle $<10^{-3}$) the mutual interference can be easily managed, using simple techniques as the above-referenced *logic AND canceller*, in SS marine radars (whose duty cycle is typically of the order of 5 up to 15%) such a canceller strongly reduces the detection probability. Summing up, the driving factor is the integrated duty cycle of the radars in visibility area of the 'victim' radar, as well as its pulse width.

Keeping in mind the above assumption, the probability of detection p_d has been defined as the complementary of the P_{Int} which is the probability of at least one interfering ship in a given time-slot T_{over}. From Figs. 4 and 5, it results that a few interfering ships, also for a low duty cycle, drastically reduce the p_d under the IMO limit of 0.8, especially when victim is a SS radar.

Pertaining solutions to this problem are not easily found. In the general radar (and radio communications) context, interference is dealt with by *diversity* in one or more parameters: frequency, space, time, polarisation and code. For the problem at hand, the limited band allocated to marine radars, associated with the relatively wide band of their high-resolution and short-range operating modes and with the lack of coordination between vessels concerning radar operation, does not show many potential for frequency multiplexing. The same applies of course to the emission time. Concerning the space parameter, the usage of ultra-low side lobes antennae could limit interferences to the main lobe, but the cost of these antennae is likely out of the budget of the marine market. Polarisation diversity only permits to radiate pairs of orthogonal signals, and the same applies to up and down chirp codes, while the traffic analysis presented before

underlines the need here for $N-$ places (with $N \gg 1$, order of tens), not pairs, of orthogonal signals. Noise radar technology is a way being investigated to try to mitigate the problem presented in this paper, see [15–18]. However, the related costs are probably beyond the affordable costs for simple radar sets on board of fishing or leisure boats; therefore we are studying some innovative marine radar architectures to be presented in future works.

On the other hand, the effect of interfering radar signals on the detection performance of SS or MG marine (navigation) radars depends on many variables difficult to model, mainly related to the environment and to the specific conditions of the vessel traffic [14]. Let us consider two radars (assumed equal just for the sake of simplicity), i.e. the own and the interfering one: in clear space, line-of-sight propagation, ideal transmission/reception by the antenna main lobe only, the 'ideal' power ratio – in the same operating band – between the interfering signal and the radar echo of the ship having a given radar cross-section σ at distance R is simply $4\pi R^2/\sigma$. The antenna sidelobes and the filtering in reception may attenuate the interference by a figure denoted A, so the ratio becomes $4\pi AR^2/\sigma$. Both power levels are equal (i.e. echo = interference) for $\sigma = 10\ \mathrm{m}^2$ when the interference is attenuated by 60 dB and R is less than about half a nautical mile or when the interference is attenuated by 90 dB and R is less than about 15 nautical miles, a value close to the radar horizon or above it, in many practical navigation radar installations (see Table 2). Even including the attenuation by the antenna sidelobes (say, 50 dB considering both antennae), the needed additional 40 dB attenuation can be achieved in principle by frequency selectivity. However, the scope would be very limited due to the narrow available band width (200 MHz) and to the relatively wide band needed for the required range resolution (i.e. 20 MHz needed for the requested 7.5 m resolution), not to mention the wide band occupied by the MG transmitters (normally, from 9.38 to 9.44 MHz for the 'nominal' 9410 MHz commercial MGs), leaving not more than four frequency channels (e.g. at 9310, 9340, 9450 and 9490 MHz) to SS marine radars and two (at 9375 and 9410 MHz) to the MG ones (see Fig. 6).

Finally, the results shown here will be refined in future studies adding a more complete model of the 'victim' radar receiver taking into account the multipath effects, the antenna patterns as well as its rotation. Also the marine environment here leading to the gamma model should be better detailed concerning the difference between '*in-harbour*' and '*enroute*' state of the vessels. Such studies could be aimed to suggest new regulations (e.g. posing a duty cycle limit) as well as new architecture for the next generation marine radars.

6 Acknowledgments

Special thanks were due to C.V. Giuseppe Aulicino and to S.T.V. Antonio Vollero from the Italian Coast Guard for their collaboration and for providing AIS data of vessel traffic.

7 References

1 International Maritime Organization (IMO) Document: 'International Convention for the Safety Of Life At Sea'. (SOLAS). Lloyd's register, 07/2002
2 IMO, Resolution MSC.192(79) on: 'Adoption of the revised performance standards for radar equipment', 12/2004
3 Recommendation ITU-R M.1313-1: 'On technical characteristics of maritime radionavigazion radars', 2000
4 Briggs, J.N.: 'Target detection by Marine Radar' (Michael Faraday House, London, 2004)
5 Harman, S.: 'The performance of a novel three-pulse radar waveform for marine radar system'. Proc. of the 5th EuRad Conf. 2008, Amsterdam, the Netherlands, October 2008, pp. 160–163
6 Skolnik, M.I.: 'Introduction to radar systems' (McGraw-Hill, 2001, 3rd edn.)
7 'Marine Traffic', http://www.marinetraffic.com
8 'Ship Finder', http://www.shipfinder.co
9 'Ship Spotting', http://www.shipspotting.com
10 Papoulis, A.: 'Probability and statistics' (Prentice-Hall, 1990)
11 Abramowitz, M., Stegun, I.A.: 'Handbook of mathematical functions' (Dover Publications, New York, 1964)
12 Galati, G., Guarguaglini, P.F.: 'A mathematical model for the binary moving window extractor analysis', *Alta Frequenza N. 4*, 1977, XLVI, pp. 187-97E–191-101E
13 Barton, D.K.: 'Radar system analysis and modelling' (Artech House, 2005)
14 Galati, G., Pavan, G.: 'Mutual interference problems related to the evolution of marine radars'. ITSC 2015, IEEE Int. Conf. on Intelligent Transportation Systems, Canaries Islands, 15–18 September 2015
15 Galati, G.: 'Coherent radar'. International Patent PCT/IB2014/061454, 15 May 2014
16 Kulpa, K.: 'Signal processing in noise waveform radar' (Artech House, 2013)
17 Galati, G., Pavan, G., De Palo, F.: 'Generation of pseudo-random sequences for noise radar applications'. Proc. of 15th IRS 2014, Gdansk, Poland, 2014, vol. 1, pp. 115–118, doi: 10.1109/IRS.2014.6869189
18 De Palo, F., Galati, G.: 'Orthogonal waveforms for multiradar and MIMO radar using noise radar technology'. Signal Processing Symp. (SPSympo) 2015, Dębe (Poland), 10–12 June 2015, doi: 10.1109/SPS.2015.7168272

8 Appendix: Interference mitigation by increase of the threshold *M* of the moving window

It has been mentioned before that the binary moving window extractor is advantageous (with respect to multi-bit extractors as well as to some forms of coherent integration) when pulsed interferences are present and that this advantage may be exploited increasing the threshold M. As a matter of fact, the binary integration in intrinsically more robust concerning the P_{FA} with respect to the effect of the interferences. However, from the performed analysis (Fig. 9 shows the case of the optimum M), it results that, also in this case, the IMO detection requirements, in particular that of $P_{FA} \leq 10^{-4}$, are not satisfied in an interfered environment even for small values (<0.05) of the probability of interference.

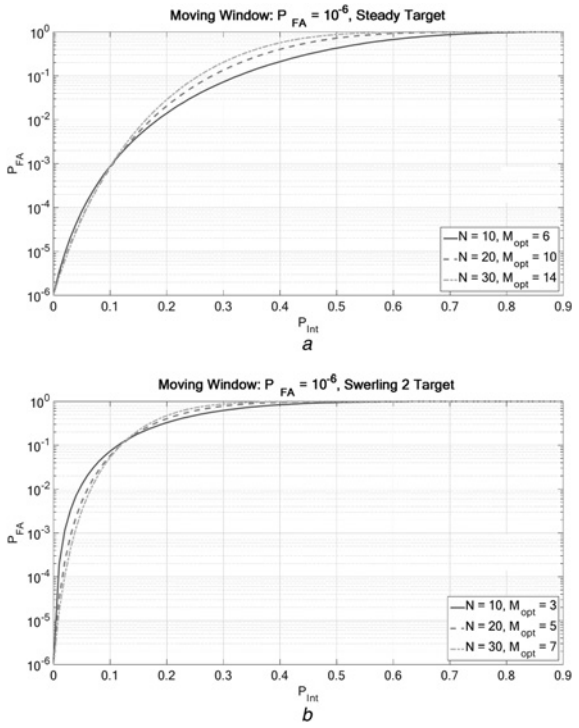

Fig. 9 *Probability of false alarm after integration against the probability of interference*

a Non-fluctuating target (steady target)
b Fluctuating target: Swerling 2